






Structural properties of charged compact stars with color-flavour-locked quarks matter

M. K. Jasim ^{1,*} Anirudh Pradhan ^{2,†} Ayan Banerjee ^{3,‡} Takol Tangphati ^{4,§} and Grigoris Panotopoulos ^{5,6,¶}

¹*Department of Mathematical and Physical Sciences, College of Arts and Sciences, University of Nizwa, Nizwa, Sultanate of Oman*

²*Department of Mathematics, Institute of Applied Sciences and Humanities, GLA University, Mathura-281 406, Uttar Pradesh, India*

³*Astrophysics and Cosmology Research Unit, School of Mathematics, Statistics and Computer Science, University of KwaZulu-Natal, Private Bag X54001, Durban 4000, South Africa*

⁴*Department of Physics, Faculty of Science, Chulalongkorn University, Bangkok 10330, Thailand*

⁵*Centro de Astrofísica e Gravitação-CENTRA, Instituto Superior Técnico-IST, Universidade de Lisboa-UL, Av. Rovisco Pais, 1049-001 Lisboa, Portugal*

⁶*Departamento de Ciencias Físicas, Universidad de la Frontera, Casilla 54-D, 4811186 Temuco, Chile*

(Dated: October 8, 2021)

The observations of pulsars with masses close to $2M_{\odot}$ have put strong constraints on the equation of state (EoS) of neutron-rich matter at supranuclear densities. Moreover, the exact internal composition of those objects is largely unknown to us. Aiming to reach the $2M_{\odot}$ limit, here we investigate the impact of electric charge on properties of compact stars assuming that the charge distribution is proportional to the mass density. The study is carried out by solving the Tolman-Oppenheimer-Volkoff (TOV) equation for a well-motivated exotic quark matter in the color-flavor-locked (CFL) phase of color superconductivity. The existence of the CFL phase may be the true ground state of hadronic matter with the possibility of the existence of a pure stable quark star (QS). Concerning the equation-of-state, we obtain structural properties of quark stars and compute the mass, the radius as well as the total electric charge of the star. We analyze the dependence of the physical properties of these Qs depending on the free parameters with special attention on mass-radius relation. We also briefly discuss the mass vs central mass density ($M - \epsilon_c$) relation for stability, the effect of electric charge and compactness. Finally, our results are compared with the recent observations data on mass-radius relationship.

I. INTRODUCTION

Compact stars including neutron stars (NSs) and quark stars (Qs) are excellent test-beds to probe their internal composition and nature of particle interactions at extremely high density regime. In turn, this would provide us with a very precise description of the internal structure, allowing an equation-of-state (EoS) (i.e. the relation between pressure and density) at nuclear and supra-nuclear densities that can provide clues to the interactions between elementary particles as well. Many such theoretical EoSs have been proposed, ranging from ‘soft’—a mass upper limit as low as $1.5 M_{\odot}$ [1] to ‘stiff’—a higher upper mass limit near $3M_{\odot}$ [2]. Thus, the accurate measurement of mass-radius relation and corre-

sponding maximum mass of compact stars is important for our understanding of the EoS of matter in such high-density situations.

Presently, we have most reliable observational constraints on the properties of the maximum-mass NSs coming from high-precision x-ray space missions, such as the Neutron Star Interior Composition Explorer (NICER) [3, 4] and enhanced X-ray Timing and Polarimetry mission (eXTP) [5] are potentially even more informative. The most recent and major breakthrough came from the first NICER simultaneous mass and radius measurement of the millisecond pulsar PSR J0030+0451 [6, 7]. This high-quality data presently put a very strong lower limit on the maximum mass, and have already ruled out many soft EoSs. Meanwhile, the LIGO and Virgo Collaborations have announced that the gravitational wave event GW 190814 [9] indicate the existence of a compact binary merger with a $(22.2 - 24.3) M_{\odot}$ black hole and a compact object with a mass at $(2.50 - 2.67) M_{\odot}$. The event GW 190814 provides us with an unprecedented probe into the mass gap between NSs and

* Email:mahmoodkhalid@unizwa.edu.om

† Email:pradhan.anirudh@gmail.com

‡ Email:ayanbanerjeemath@gmail.com

§ Email:takoltang@gmail.com

¶ Email:grigorios.panotopoulos@ufrontera.cl

BHs. Thus, the secondary component of the event GW 190814 is the most massive NS discovered to date, and this can be explained either within GR or within alternative theories of gravity, see e.g. [10–14].

On the other hand, our theoretical and observational knowledge about NSs put a strong constraint on the theoretical models of dense nuclear matter, after the discovery of pulsars with $\sim 2 M_{\odot}$ including the binary millisecond pulsar J1614-2230, with mass $1.928 \pm 0.017 M_{\odot}$ [4], and the pulsar J0348+0432 with mass $2.01 \pm 0.04 M_{\odot}$ [8]. The latest record is held by PSR J0740+6620, a millisecond pulsar having an updated mass of $2.08 \pm 0.07 M_{\odot}$ with its predicted radius 12.35 ± 0.75 [15] provide us a totally new avenue to probe the internal structure of NS. Recently, two independent analyses by NICER and XMM-Newton Data found the radius to be $12.39^{+1.30}_{-0.98}$ km [16] or $13.7^{+2.6}_{-1.5}$ km [17] at 68% confidence. Additionally, a new constraint $R(1.6 M_{\odot}) > 10.7$ km has been set from the analysis of the tidal deformability obtained from GW 170817 [18]. All these measurements are more reliable than traditional spectroscopic measurements, and provide key input to analyse the NS structure and corresponding EoS.

As a consequence a lot of effort has been put forward to resolve that problem over the last couple of decades, but the final answer is still missing up to this day. With this issue the possible existence of quark matter in compact stars has attracted the attention for decades. Initially it was pointed out in [19, 20] that compact stars are partially or totally made of quarks. However, according to the strange quark matter (SQM) hypothesis, this form of matter is constituted of almost equal numbers of u , d and s , with the s quark number slightly smaller due to its relatively higher static mass. It has been conjectured that SQM may be the absolute ground state of strongly interacting matter [20, 21], as its energy per baryon could be less than that of the most stable atomic nucleus, such as ^{56}Fe and ^{62}Ni .

As a result, there are several models used to approach the strange matter hypothesis, and the MIT Bag Model is one of the most successful ones for quark confinement. Based on this model several authors have shown the stability of strange matter [22–24], which processes many desirable features inspired by Quantum Chromodynamics (QCD) and relativity. On the other hand, the present knowledge of QCD suggests that quark matter might be in different color superconducting phases where the temperature is low and the density is high enough, see Ref. [25–27] for details. As a result, several authors have considered an even more extreme possibility depending on the details of the quark-quark interaction, such as two-flavor color superconductor (2SC)

[28, 29], the color-flavor locked (CFL) phase [30, 31], and interacting quark EoS at ultra-high densities [32–34].

Most of the investigations have been done under the assumption of the electric charge neutrality inside the fluid sphere. But, this point of view had been challenged by several researchers [35, 36]. According to them the matter acquires large amounts of electric charge during the gravitational collapse or during an accretion process onto a compact object. This point has been discussed in [37, 38]. Moreover, the presence of electrons play a crucial role in the formation of an electric dipole layer on the surfaces of compact stars that lead to huge electric fields of order 10^{18} V/cm [39, 40]. In general, a net electric charge on compact stars may induce intense electric fields, whose effects will add up to the internal pressure of the system. The overall repulsive force will overwhelm the gravitational one, which implies that electrically charged stars can be more stable than their neutral counterparts. In this spirit electric charge in compact stars have widely been accepted among researcher, see Refs. [41, 42] and references therein. However, in the stellar configuration, charge can be as high as 10^{20} Coulomb to bring in any change in the mass-radius relation [43]. The situation is even more extreme if strange stars were made of interacting quark EoS [44].

Furthermore, we find several astrophysical model with huge amounts of charge. In Ref. [45], author has studied the charged perfect fluid solutions assuming a linear equation-of-state. The resulting solution brings several consequences including charged isotropic and anisotropic fluid solutions for linear or non-linear EoS [46–50] as well. Also, many works have been done to explore the idea of strong electric field [51, 52] in the presence of strange matter followed by the MIT bag model EoS. The most notable technique for the analysis of stability against radial perturbation has been studied for charged strange quark stars [51]. Solutions of the Einstein-Maxwell system of equations for static spherically symmetric interior spacetimes were also investigated in Refs. [53–55].

Thus, the effect of electric charge on compact objects is of great interest. In this work, we will focus on the structure properties of a charged sphere assuming the EoS for CFL strange quark matter. Obtained mass-radius relations predicted by the theory, we also compare them with existing observational constraints like NICER measurement of PSR J0740+6620 [15], PSR J0348+0432 [8], EXO 1745-248 [56], PSR J0751+1807 [57] and PSR J0030+0451 [7]. This paper is organized as follows: in Sec. II, we shortly discuss the Einstein-Maxwell system of equations for static spherically symmetric spacetime. In Sec. III we present the boundary

conditions and explain the method used for the numerical integration of the equations. In Sec. IV we discuss the EoS for CFL strange quark matter. To simplify our calculation we assume that charge density is proportional to the energy density. In Sec. V, we present the numerically obtained results for quark matter stars by solving the TOV equations. Subsequently, we discuss the mass-radius relation and the stability of hydrostatic equilibrium. We close with a brief discussion of the results in Sec. VI. Throughout we use a system of units in which $G = c = 1$ and choose the sign conventions $(+, -, -, -)$

II. GENERAL RELATIVISTIC SELLAR STRUCTURE

To begin with the construction, let us start by considering the static spherically symmetric metric, which is specified by the line element ($ds^2 = g_{\nu\mu}dx^\nu dx^\mu$, where $\nu, \mu = 0, 1, 2, 3$),

$$ds^2 = e^{\Phi(r)} dt^2 - e^{\Lambda(r)} dr^2 - r^2 d\Omega^2, \quad (1)$$

where $d\Omega^2 = d\theta^2 + \sin^2\theta d\varphi^2$ is the line element on the unit 2-sphere with two unknown functions $\Phi(r)$ and $\Lambda(r)$, respectively.

The stress-energy tensor $T_{\nu}{}^{\mu}$, which in the present study is written as $T_{\nu}{}^{\mu} = M_{\nu}{}^{\mu} + E_{\nu}{}^{\mu}$. The sum of two terms associate with a perfect fluid source and the electromagnetic term,

$$T_{\nu}{}^{\mu} = (\epsilon + P)u_{\nu}u^{\mu} + P\delta_{\nu}{}^{\mu} + \frac{1}{4\pi} \left(F^{\mu l} F_{\nu l} + \frac{1}{4\pi} \delta_{\nu}{}^{\mu} F_{kl} F^{kl} \right). \quad (2)$$

Here $\epsilon(r)$, $P(r)$ and u^{μ} are the energy density, the pressure, and the four-velocity of the fluid, respectively. In addition to this the electromagnetic field tensor $F^{\nu\mu}$ satisfy the covariant Maxwell equations

$$[(-g)^{1/2} F^{\nu\mu}]_{,\mu} = 4\pi j^{\nu} (-g)^{1/2}, \quad (3)$$

where j^{μ} is the 4-current density. Since the present choice of the electromagnetic field is only due to charge, thus all components of the electromagnetic field tensor vanish, except the radial component of the electric field F^{01} which satisfy $F^{01} = -F^{10}$. Hence, the only non-vanishing component of Maxwell equations (3) is given by

$$E(r) = F^{01}(r) = \frac{1}{r^2} e^{-(\Phi+\Lambda)/2} 4\pi \int_0^r r'^2 \rho_{ch} e^{\Lambda/2} dr', \quad (4)$$

where $\rho_{ch} = e^{\Phi/2} j^0(r)$ is the electric charge distribution inside the star. The final expression (3) is given by

$$\frac{dq(r)}{dr} = 4\pi r^2 \rho_{ch} e^{\Lambda/2}. \quad (5)$$

Thus, one can get the full expression for energy-momentum tensor of Eq. (2), which yield

$$T_{\nu}{}^{\mu} = \begin{pmatrix} \epsilon + \frac{q^2}{8\pi r^4} & 0 & 0 & 0 \\ 0 & -P + \frac{q^2}{8\pi r^4} & 0 & 0 \\ 0 & 0 & -P - \frac{q^2}{8\pi r^4} & 0 \\ 0 & 0 & 0 & -P - \frac{q^2}{8\pi r^4} \end{pmatrix}, \quad (6)$$

where the electric charge is connected to the electric field through the relation $q(r)/r^2 = E(r)$. The (tt) and (rr) components of the Einstein-Maxwell equations for the metric (1) and the energy-momentum tensor (2) are then given by

$$e^{-\Lambda} \left(\frac{1}{r} \frac{d\Lambda}{dr} - \frac{1}{r^2} \right) + \frac{1}{r^2} = 8\pi \left(\epsilon + \frac{q^2(r)}{8\pi r^4} \right), \quad (7)$$

$$e^{-\Lambda} \left(\frac{1}{r} \frac{d\Phi}{dr} + \frac{1}{r^2} \right) - \frac{1}{r^2} = 8\pi \left(P - \frac{q^2(r)}{8\pi r^4} \right). \quad (8)$$

Here, we introduce the gravitational mass $m(r)$ inside the sphere of radius r is given by

$$e^{-\Lambda(r)} \equiv 1 - \frac{2m(r)}{r} + \frac{q^2(r)}{r^2}. \quad (9)$$

Using the Eq. (9), this equation (7) gives [58, 59]

$$\frac{dm}{dr} = 4\pi r^2 \epsilon + \frac{q}{r} \frac{dq}{dr}. \quad (10)$$

Note that the sum of two terms on the right hand side of Eq. (10) corresponds to the mass-energy of the stellar matter and the mass-energy of the electric field carried the electrically charged star. Moreover, from the Bianchi identities $\nabla_{\nu} T_{\mu}{}^{\nu} = 0$, it follows

$$\frac{d\Phi}{dr} = -\frac{2}{(\epsilon + P)} \left(\frac{dP}{dr} - \frac{q}{4\pi r^4} \frac{dq}{dr} \right). \quad (11)$$

Then, replacing (5) and taking into account the expressions (11) into Eq. (8), we get

$$\frac{dP}{dr} = -\frac{2 \left(m + 4\pi r^3 \left(P - \frac{q^2}{4\pi r^4} \right) \right)}{r^2 \left(1 - \frac{2m}{r} + \frac{q^2}{r^2} \right)} (P + \epsilon) + \frac{q}{4\pi r^4} \frac{dq}{dr}, \quad (12)$$

which is the Tolman-Oppenheimer-Volkoff (TOV) equation for an electrically charged fluid sphere. For $q \rightarrow 0$ these equations reduce to the ordinary TOV equations of General Relativity for electrically neutral fluid spheres.

Thus, we have six unknown functions– $\Phi(r)$, $m(r)$, $q(r)$, $\epsilon(r)$, $P(r)$ and $\rho_{ch}(r)$, for which there are four equations, (5), (10), (11) and (12). Therefore, the above system of equations is under-determined, and we will reduce the number of unknown functions by assuming suitable conditions for charged fluid sphere (see [51, 60] for more details). In particular, one may consider a relation between the pressure and the density is called the equation-of-state, which is necessary to solve the equations for the stellar structure of the star. Furthermore, a linear relation between the charge distribution and the mass density will be assumed in order to solve the system of structure equations, combined with the appropriate boundary conditions.

III. BOUNDARY CONDITIONS AND THE EXTERIOR VACUUM REGION

The main aim here is to numerically solve the modified TOV equations inside and outside the star simultaneously for the sought solutions. In the present case, we maintain the regularity inside the fluid sphere with the following boundary conditions:

$$\begin{aligned} m(r=0) = 0, \quad q(r=0) = 0, \quad \epsilon(r=0) = \epsilon_c, \quad (13) \\ P(r=0) = P_c, \quad e^{\Lambda(r)}|_{r=0} = 1, \quad \text{and} \quad P(R)|_{r=R} = 0, \end{aligned}$$

where $r = R$ is the surface of the star with P_c is the central pressure and ϵ_c is the central energy density, respectively. As our aim is to solve the TOV equations numerically for a specific EoS, here we choose an appropriate set of boundary conditions. We start with a central density ϵ_c , and a corresponding central pressure P_c , and then integrate towards the surface where the pressure vanishes.

On the other hand, our numerical solution should match the external solution for $r > R$. The unique solution to the Einstein-Maxwell system for $r > R$ is given by the Reissner-Nordström spacetime,

$$ds^2 = F(r)dt^2 - \frac{dr^2}{F(r)} - r^2 d\Omega^2 \quad (14)$$

where $F(r) = \left(1 - \frac{2M}{r} + \frac{Q^2}{r^2}\right)$. By matching the solution we can find the total mass M and the total charge Q of the star. Since, the first fundamental form at the boundary implies that $g_{tt}^- = g_{tt}^+$ and $g_{rr}^- = g_{rr}^+$, which implies

$$e^{\Phi(r)}|_{r=R} = F(R) \quad \text{and} \quad e^{-\Lambda(r)}|_{r=R} = F(R), \quad (15)$$

with other conditions are $m(R) = M$ and $q(R) = Q$, besides $P(R) = 0$.

IV. EQUATIONS OF STATE FOR QUARK MATTER AND THE CHARGE DENSITY PROFILE

A. Specific equations-of-state

As mentioned before, we have two degrees of freedom. Thus, we need to specify an EoS and an assumption for the charge density, as the matter content carries a net electric charge. First, we define the standard relations between pressure and energy density through the EoS. We work here within the hypothesis that quark matter is absolutely stable and thus quark stars contain roughly equal numbers of up, down, and strange quarks. Moreover, strange quark matter (SQM) is supposed to be the most stable quantum state of the hadronic matter [19, 20].

On the other hand, color superconductivity in quark matter has become a compelling topic that devoted to the physics of compact star interiors. At sufficiently large densities and low temperatures that hadrons are crushed into quark matter, there is a whole family of ‘‘color superconducting’’ phases [61–63]. The rich phase structure is essentially due to the quark-quark interaction. Since, the interaction is strong and attractive in many channels with the possibility of many degrees of freedom for quarks like color, flavor and spin so that various kinds of BCS pairing are possible. With this assumption several models have been predicted in existence of a large variety of color superconducting states of quark matter at ultra-high densities [25–27].

In the present work we focus on the three-flavor quark matter with the particular symmetry is called the color-flavor locked matter at asymptotically high density. It is widely accepted that the CFL phase is the real ground state of QCD at asymptotically large densities. Quark matter in the CFL phase is electrically neutral, and electrons cannot be present, contrary to the case of NSs where neutrality requires the presence of electrons. When the color superconducting pairing is considered in the CFL phase, the thermodynamic potential for electric and color charge neutral CFL quark matter to order Δ^2 is given by [64]

$$\begin{aligned} \Omega_{CFL} = & -\frac{3\Delta^2\mu^2}{\pi^2} + \frac{6}{\pi^2} \int_0^{\gamma_F} p^2(p-\mu) dp \\ & + \frac{3}{\pi^2} \int_0^{\gamma_F} p^2 \left(\sqrt{p^2 + m_s^2} - \mu \right) dp + B, \quad (16) \end{aligned}$$

where μ is the quark chemical potential and Δ denotes the color superconducting gap parameter of the CFL phase of quark matter. The first term is the contribution of the CFL condensate to Ω_{CFL} , and the next two terms coming from the thermodynamic potential of (fictional)

unpaired quark matter in which all quarks that are going to pair have a common Fermi momentum γ_F , with γ_F chosen to minimize the thermodynamic potential of the fictional unpaired quark matter [65]. The final term is the bag constant.

The common Fermi momentum γ_F is given by

$$\gamma_F = \left[\left(2\mu - \sqrt{\mu^2 + \frac{m_s^2 - m_u^2}{3}} \right)^2 - m_u^2 \right]^{1/2} \quad (17)$$

where $\mu = (\mu_s + \mu_u + \mu_d)/3$ is the average quark chemical potential, and m_s and m_u are strange and up quark masses, respectively. For massless up and down quarks we get

$$\gamma_F = 2\mu - \sqrt{\mu^2 + \frac{m_s^2}{3}} \sim \mu - \frac{m_s^2}{6\mu}. \quad (18)$$

With the pairing ansatz in the CFL phase [31]

$$n_u = n_r, \quad n_d = n_g, \quad \text{and} \quad n_s = n_b \quad (19)$$

where n_r, n_g, n_b and n_u, n_d, n_s are color and flavor number densities respectively. The pressure, baryon number density n_B , and particle number densities are easily derived and read

$$P = -\Omega_{CFL} \quad \text{and} \quad n_u = n_d = n_s = \frac{\gamma_F^3 + 2\Delta^2\mu}{\pi^2}. \quad (20)$$

Since we work at zero temperature, the energy density is given by [66]

$$\epsilon = 3\mu n_B - P. \quad (21)$$

Note that in the limit $m_s \rightarrow 0$ the particle densities become equal, and the EoS takes the simple form $\epsilon = 3P + 4B$. Pairing introduces the Δ^2 term in Eq. (16); thus the EoS picks up an extra term from CFL contribution as $\epsilon = 3P + 4B - 6\Delta^2\mu^2/\pi^2$. However, this situation becomes more complicated and difficult to obtain an exact expression for an EoS when $m_s \neq 0$. Thus, the series upto the order Δ^2 and m_s^2 helps us to keep the EoS very simple and useful for most calculations, which yield [67]

$$P = \frac{3\mu^4}{4\pi^2} + \frac{9\beta\mu^2}{2\pi^2} - B, \quad (22)$$

$$\epsilon = \frac{9\mu^4}{4\pi^2} + \frac{9\beta\mu^2}{2\pi^2} + B, \quad (23)$$

where

$$\beta = -\frac{m_s^2}{6} + \frac{2\Delta^2}{3}. \quad (24)$$

From the above expressions we can obtain an analytic expression for $\epsilon = \epsilon(P)$:

$$\epsilon = 3P + 4B - \frac{9\beta}{\pi^2} \left\{ \left[\frac{4\pi^2(B+P)}{3} + 9\beta^2 \right]^{1/2} - 3\beta \right\}. \quad (25)$$

Since the case of Eq. (25) contains three free parameters which are m_s , Δ and B , respectively. In this work, we choose the values of the color superconducting gap $\Delta \sim 50 - 150$ MeV, see Refs. [68, 69]. In order to be absolutely stable the energy per baryon of the CFL phase, the bag constant B always to be greater than 57 MeV/fm³ [70] and the strange quark mass m_s to be $m_s \sim 50 - 150$ MeV. We use all the values for our QS which fall inside the *stability windows* presented in Ref. [71].

B. The charge density relation

We also need to specify the charge density as the matter field carries a net electric charge. As discussed in [43, 60], we assume that the charge density is proportional to the energy density, i.e.

$$\rho_{ch} = \alpha \epsilon, \quad (26)$$

with α being the charge fraction. This is a reasonable assumption in the sense that large mass can hold large amount of charge. Moreover,

$$\frac{Q}{M} = \frac{\rho_{ch}}{\epsilon} = \alpha, \quad (27)$$

and since for the RN solution $Q \leq M$, the charge fraction lies in the range of $0 \leq \alpha \leq 1$.

V. NUMERICAL RESULTS

In this section we present our main numerical results for the given EoS which was discussed in Sec. IV. To get a good estimate of how quark stars might be, we vary Δ , charge fraction α , the bag constant B and the strange quark mass m_s , over a physically reasonable range and calculate the mass-radius relations in each case. Here, the mass of the star is measured in units of solar masses M_\odot , the radius of the stars in Km, the total electric charge in C (Coulomb), while the energy density, the pressure and the bag constant are expressed in MeV/fm³. In the following analysis we discuss four sets of solutions (i) variation of color superconducting gap $\Delta = (50 - 150)$ MeV, (ii) variation of α in the range of $\alpha \approx (0 - 1)$, (iii) variation of bag constant $B = (57 - 92)$ MeV/fm³, and (iv) variation of the strange quark mass $m_s = (50 - 150)$ MeV, respectively. The results of our calculations are displayed in five distinct Tables I-V, respectively.

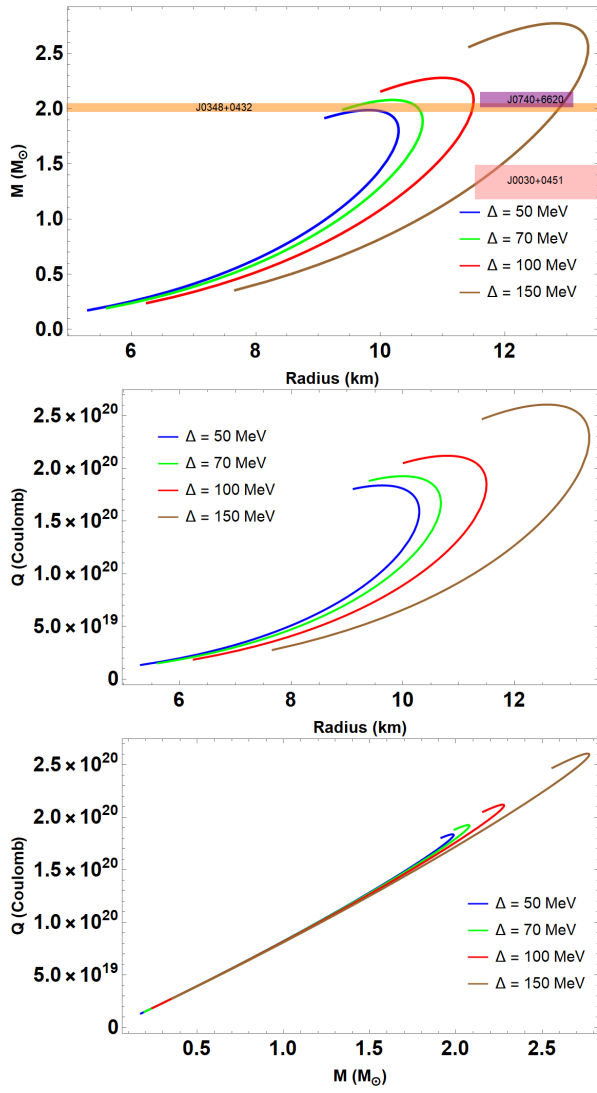


FIG. 1. The top panel shows the behavior of the mass-radius relation, while the one in the middle shows the variation of the total charge with the radius. The bottom panel shows the variation of the charge with the mass for different $\Delta = 50, 70, 100, 135$ MeV. For plotting we set the other parameters $B = 70$ MeV/fm³, $m_s = 150$ MeV and $\alpha = 0.43462$, respectively. The horizontal bands show the observational constraints from various pulsar measurements: PSR J0348+0432 (Orange) [8], PSR J0740+6620 (Purple) [15] and GW 190814 event with the mass range 2.50 - $2.67 M_\odot$ (Yellow) [9], see text for details.

A. Mass-Radius relation

We have obtained the $M - R$, $Q - R$ and $Q - M$ relations for some values of the central pressure with a fixed value of $\alpha = 0.43462$ and different values of $\Delta = (50, 70, 100, 135)$ MeV. The upper panel of Fig. 1 shows that the maximum mass of the quark star exceeds the $2M_\odot$ for $\Delta > 50$ MeV. For a given mass the radius

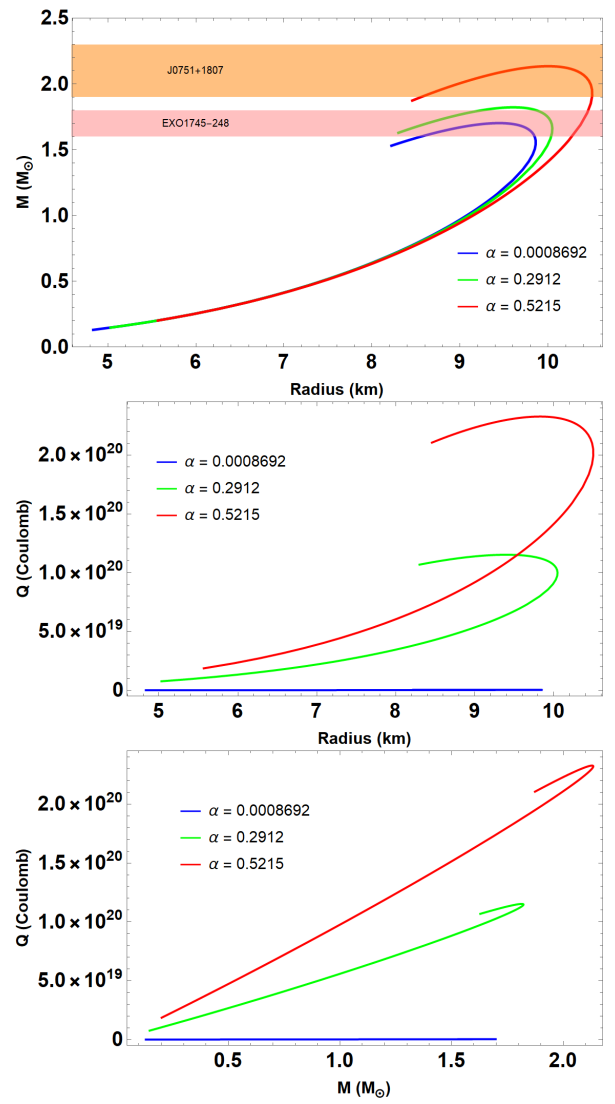


FIG. 2. We maintain the same sequence as of Fig. 1. The stars described by the EoS (25) with $B = 70$ MeV/fm³, $m_s = 150$ MeV, $\Delta = 50$ MeV and different values of $\alpha = 0.0008692, 0.2912, 0.6954$, respectively. The three horizontal bands show the observational constraints from EXO 1745-248 (Pink) [56], PSR J0751+1807 (Orange) [57] and GW 190814 event with the mass range 2.50 - $2.67 M_\odot$ (Yellow) [9].

increases with Δ , and therefore the factor of compactness, $C = M/R$, decreases with Δ . The same conclusion is reached looking at the lower panel of Fig. 5. Furthermore, it is clear from panels 1 and 3 of Fig. 1 that the highest mass and the corresponding radius of the stars increase with Δ , see Table I. This is due to the effect of the repulsive force that a charged star has, and supports the existence of more massive stars avoiding the gravitational collapse. The slope of the $Q - M$ curves come from the different color superconducting gap. In panel 2, we show the $Q - R$ diagram for some values

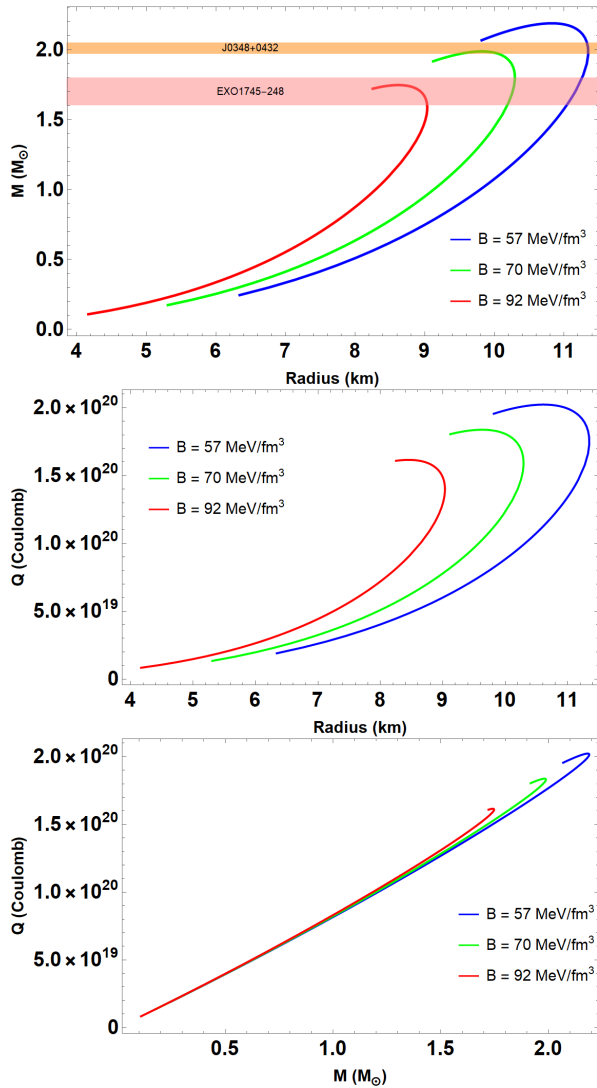


FIG. 3. We repeat the same sequence as of Fig. 1 for the set parameters $\Delta = 50$ MeV, $m_s = 150$ MeV, $\alpha = 0.43462$ and different values of $B = (57, 70, 92)$ MeV/fm³. The horizontal bands indicate the masses of PSR J0348+0432 [8] and EXO 1745-248 [56] pulsars.

of Δ . Notice that the total charge increases with the total mass until it reaches the point of maximum charge value. With the knowledge of the mass-radius relations predicted by different astrophysical groups, our findings are compatible with the existence of the massive pulsars PSR J0740+6620 having a mass of $2.08 \pm 0.07 M_\odot$ with its predicted radius 12.35 ± 0.75 (Purple) [15], PSR J0348+0432 with $2.01 \pm 0.04 M_\odot$ (Orange) [8] and GW 190814 event with the mass range 2.50 - $2.67 M_\odot$ (Yellow) [9] represented by horizontal stripes in Fig. 1. In Table I, we summarize a few relevant quantities of QSs that are used in the present work and in Fig. 1.

In Fig. 2, we repeat the same sequence as of Fig. 1,

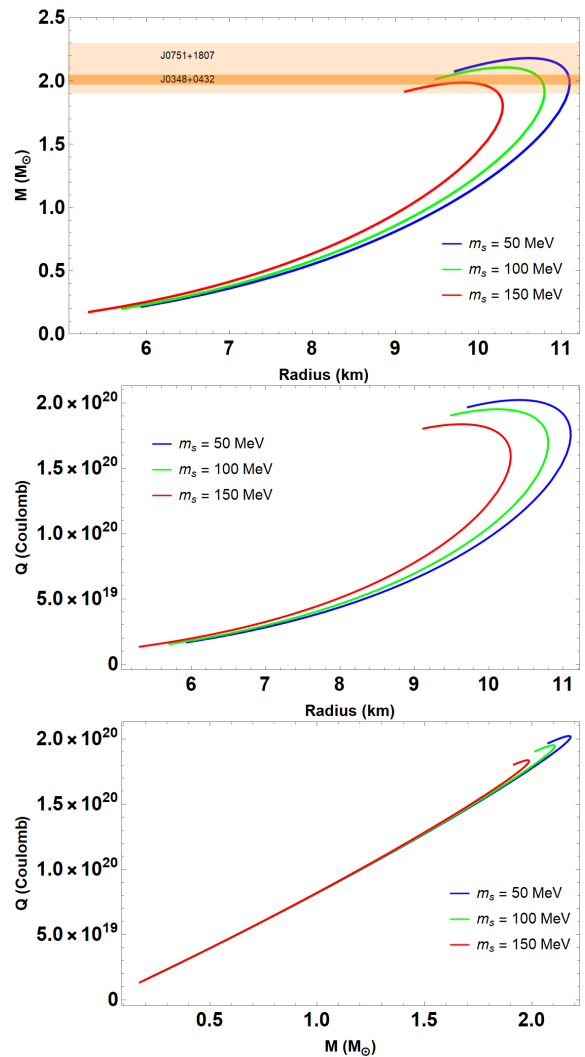


FIG. 4. Same as Fig. 1, but for the set of parameters $\Delta = 50$ MeV, $B = 70$ MeV/fm³, $\alpha = 0.43462$ and different values of $m_s = (50, 100, 150)$ MeV. The horizontal bands indicate two massive pulsars PSR J0751+1807 (Pink) [57] and PSR J0348+0432 (Orange) [8].

but this time we show the impact of α from 0.0008692 to 0.6954 on the properties of the QSs, setting $\Delta = 50$ MeV and $m_s = 150$ MeV. The shape of the profiles $M - R$ and $Q - R$ is qualitatively similar to those of Fig. 1. Similarly to that figure, the highest mass and the corresponding radius increase with α , although the factor of compactness, M/R , decreases with α , a feature observed elsewhere before, e.g. in [60]. This model provides best agreement with the pulsars PSR J0751+1807 has a mass of $2.1 \pm 0.2 M_\odot$ (Orange) [57], EXO 1745-248 with $M = 1.7 \pm 0.1 M_\odot$ (Pink) [56] and GW 190814 event with the mass range 2.50 - $2.67 M_\odot$ (Yellow) [9]. Plausible values of some parameters describing QS properties are shown in Table II below. It is evident from the Table

II that the maximum mass of QS can exceed $2 M_{\odot}$ if we increase the value of α sufficiently large.

Similarly, for plotting the Fig. 3, we take B as a phenomenological model input and choose the following three values of $B = (57, 70, 92) \text{ MeV}/\text{fm}^3$. The other set of parameters are $\Delta = 50 \text{ MeV}$, $m_s = 150 \text{ MeV}$ and $\alpha = 0.43462$, remain fixed. From Fig. 3, we can see that for less interacting quarks the maximum masses and their corresponding maximum radii have larger values. Moreover, the effect of interacting quarks has a similar trend on the $Q - R$ and $Q - M$ diagrams. In panel 3, the total charge grows with the total mass until it reaches the point of maximum charge value and then decreases with the increasing mass. The maximum mass for $B = 57 \text{ MeV}/\text{fm}^3$ is about $2.19 M_{\odot}$ and the corresponding radius of around 10.84 Km (see Table III, for more details). Notice that the model is consistent with stringent constraints on the maximum NS mass coming from PSR J0348+0432 (Orange) [8] and EXO 1745-248 (Pink) [56].

Another important quantity for this discussion is the effect of the strange quark mass m_s , which we show in Fig. 4. The diagrams $M - R$, $Q - R$ and $Q - M$ are plotted for three different values of $m_s = (50, 100, 150) \text{ MeV}$ with $\Delta = 50 \text{ MeV}$, $B = 70 \text{ MeV}/\text{fm}^3$ and $\alpha = 0.43462$, respectively. The trend of figures are almost similar to that of Fig. 3. We have allowed the range of values of $m_s = 150 \text{ MeV}$ that fall inside the stability windows to yield stars of maximum mass up to $M = 2.13 M_{\odot}$. The horizontal strips represent the observational constraints, from top to bottom the first two delimit the band from $(1.99 - 2.19) M_{\odot}$, which contains masses of the supermassive pulsars PSR J0751+1807 (Pink) [57] and PSR J0348+0432 (Orange) [8]. Table IV summarizes the maximum mass, total charge, radius and the compactness of the charged star for different values of strange quark mass m_s .

Finally, in Table V, we summarize the main aspects of the models used in this work i.e., maximum mass constraints for $1.4M_{\odot}$, $1.6M_{\odot}$ and $2.08M_{\odot}$ considered as a most sensational masses, which is used here to probe the sensitivity of our results to the constraint from observations. In particular, the CFL EoS is consistent with the $\sim 2M_{\odot}$ limit and predicts a radius of $R_{1.6} = 10.43 \text{ Km}$ for a $1.6M_{\odot}$ neutron star, which is very closed to the observation reported in [18].

B. Dynamical Stability and Compactness

We now proceed to study the stellar mass M against the central energy density ϵ_c for the four different sets of parameters as indicated in Section V A. To serve our

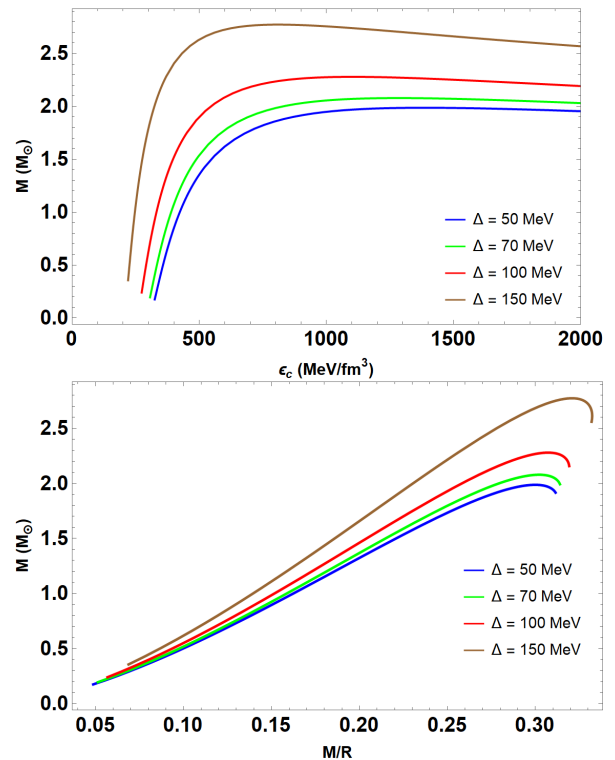


FIG. 5. The profiles of mass-energy density and compactness with the same set of parameter in Fig. 1.

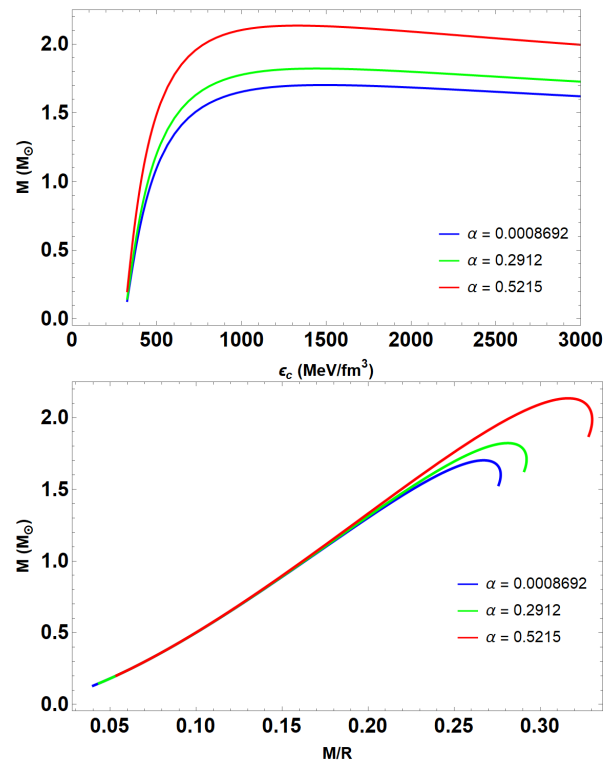


FIG. 6. The profiles of mass-energy density and compactness with the same set of parameter in Fig. 2.

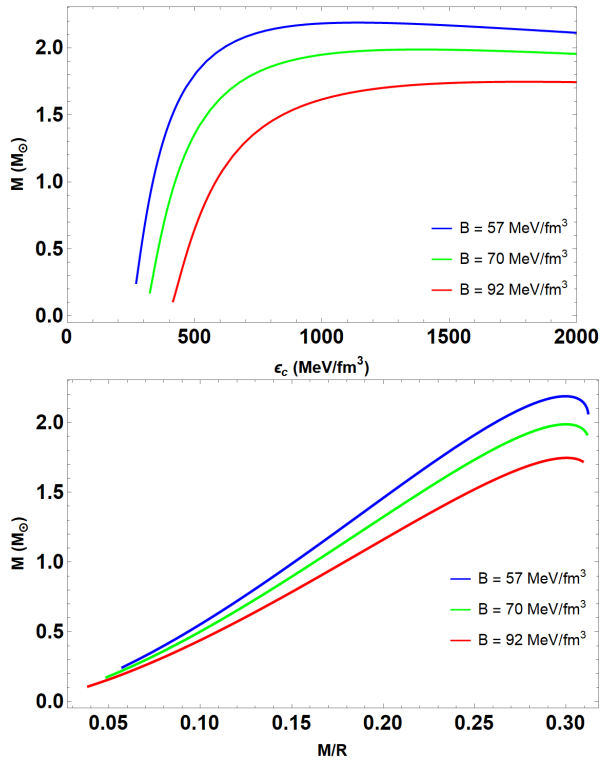


FIG. 7. The profiles of mass-energy density and compactness with the same set of parameters in Fig. 3.

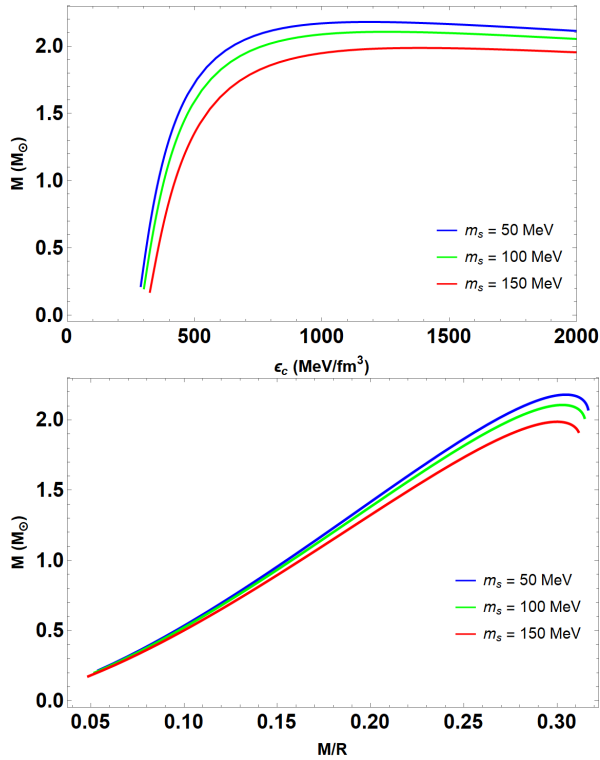


FIG. 8. The profiles of mass-energy density and compactness with the same set of parameter in Fig. 4.

purpose, we consider the so called static stability criterion [72, 73]

$$\frac{dM}{d\epsilon_c} < 0 \rightarrow \text{unstable configuration} \quad (28)$$

$$\frac{dM}{d\epsilon_c} > 0 \rightarrow \text{stable configuration,} \quad (29)$$

to be satisfied by all stellar configurations. Note that this is a necessary condition but not sufficient. The mass of the star reaches a maximum value at ϵ_c^* , which grows with the charge fraction in agreement with the $M - R$ profile in Figs. 1-4, respectively. The results have been shown in Figs. 5, 6, 7 and 8 (in the top panel), where we plot M (in solar masses M_\odot) against ϵ_c for Qs. The variation of central energy densities between the range $400 \leq \epsilon_c \leq 2000 \text{ MeV/fm}^3$. Therefore, the extremum point of the curve separates the stable from the unstable configuration.

Besides, we also analyze the compactness M/R for charged objects. The value of the ratio M/R has been shown against the maximum mass in the lower panel of Figs. 5-8, respectively. The main feature to note is that M/R decreases with increasing values of Δ and α , but M/R increases with increasing values B and m_s . Finally, we present some of the values of stellar compactness in Tables I-V. In this prescription of quark stars we found that the compactness corresponding to the highest mass increases with Δ, α, B (see Tables I, II and III for more details), and decreases with m_s (see Tables IV for more details).

In Ref. [74], Buchdahl has also obtained the compactness limit for a perfect fluid interior given by $\frac{M}{R} \leq 4/9$ for an object of mass M and radius R . The generalization of Buchdahl's bound was given for charged gravitational objects by Andréasson [75]. The limit was obtained by assuming the strong energy condition, $p_r + 2p_\perp \leq \rho$, where p_r and p_\perp are the radial and tangential pressures and ρ is the matter energy density, respectively. The Buchdahl-Andréasson bound is found to be [75, 76]

$$\frac{M}{R} \leq \frac{8}{9} \left(1 + \sqrt{1 - \frac{8Q^2}{9M^2}} \right)^{-1}. \quad (30)$$

When $Q = 0$, Eq. (30) gives the usual Buchdahl bound for electrically neutral objects, $M/R \leq 4/9$. On the other hand, when $Q = M$ we obtain for the factor of compactness the limit $M/R \leq 2/3$. For any other value of Q/M between the two extremal cases, the bound on M/R may be seen in the left panel of Figure 1 of [76]. It is clear from the Tables I-V that the star obeys the mass-radius ratio, which is a requirement of the dynamically stable horizonless charged compact object.

TABLE I. Characteristics of a set of configurations for EoS (25). We list our choices for the parameters which according to the discussion given in Fig. 1. The total charge Q of the stars is measured in Coulomb (C).

Δ	M	R	Q	ϵ_c	$\frac{M}{R}$
MeV	(M_\odot)	(Km)	($\times 10^{20}$ C)	$\frac{\text{MeV}}{\text{fm}^3}$	
50	1.99	9.83	1.83	1374	0.300
70	2.08	10.19	1.92	1295	0.302
100	2.28	11.00	2.11	1106	0.307
135	2.61	12.21	2.43	898	0.316

TABLE II. Quark star properties using the EoS (25) and their corresponding central energy densities for different values of α . We list our choices for the parameters B , m_s and Δ , which according to the discussion given in Fig. 2.

α	M	R	Q	ϵ_c	$\frac{M}{R}$
	(M_\odot)	(km)	($\times 10^{20}$ C)	$\frac{\text{MeV}}{\text{fm}^3}$	
0.000869	1.70	9.43	0.00325	1502	0.267
0.435	1.99	9.82	1.83	1380	0.300
0.695	2.59	10.50	3.59	1177	0.365

VI. CONCLUSIONS

We have studied electrically charged strange quark stars in the context of Einstein-Maxwell theory. The matter field is assumed to be color-flavor-locked (CFL) phase of color superconductivity, while the charge density is proportional to the mass density. The quark matter in the CFL phase may be the true ground state of hadronic matter with charge neutrality. Using the EoS we have solved the Tolman-Oppenheimer-Volkoff (TOV) equations, which describe hydrostatic equilibrium, together with the appropriate boundary conditions. The Reissner-Nordström spacetime has been considered to match the interior solution at the surface of the star. Finally, we explore the compatibility of Qs in the CFL phase with a set of maximum mass constraints corresponding to PSR J0740+6620, PSR J0348+0432, EXO 1745-248, PSR J0751+1807, PSR J0030+0451 and GW 190814 event with the mass range 2.50-2.67 M_\odot .

We have integrated numerically the structure equations for charged spheres, and we have explored the mass-radius ($M - R$) relation as well as some other physical properties of strange quark stars. The model adopted here is characterized by three parameters that enter into the EoS, (B , Δ , m_s), and also by the charge fraction, α , that lies in the range of $0 \leq \alpha \leq 1$. In particular, here we have explored the ($M - R$) profile based on the variation of all four free parameters of the

TABLE III. Based on the parameters of Fig. 3, we enlist the maximum-mass, total charge, radius and the compactness of the charged star with their corresponding values of central energy density.

B	M	R	Q	ϵ_c	$\frac{M}{R}$
$\frac{\text{MeV}}{\text{fm}^3}$	(M_\odot)	(Km)	($\times 10^{20}$ C)	$\frac{\text{MeV}}{\text{fm}^3}$	
57	2.19	10.84	2.01	1128	0.299
70	1.99	9.83	1.83	1374	0.300
92	1.75	8.61	1.61	1810	0.301

TABLE IV. Based on the parameters of Fig. 4, we enlist the maximum-mass, total charge, radius and the compactness of the charged star with their corresponding values of central energy density.

m_s	M	R	Q	ϵ_c	$\frac{M}{R}$
MeV	(M_\odot)	(Km)	($\times 10^{20}$ C)	$\frac{\text{MeV}}{\text{fm}^3}$	
50	2.19	10.61	2.01	1180	0.305
100	2.11	10.32	1.94	1246	0.303
150	1.99	9.83	1.83	1374	0.300

model. Our findings confirm the requirement that the EoS supports masses above $M_{\text{max}} > 2M_\odot$ depending on the choice of parameters, see Figs. 1-4. This is in agreement with the results obtained in previous similar works, where it has been observed that charged stars are more massive than their neutral counterparts.

Also, we have demonstrated the $M - \epsilon_c$ relation and compactness separately. By means of static stability criterion we infer the conditions $\frac{\partial M(\epsilon_c)}{\partial \epsilon_c} \leq 0$ that separate the stable configuration region from the unstable one at the point $(M_{\text{max}}, R_{M_{\text{max}}})$. Another interesting result in this discussion is the Buchdahl-Andréasson bounds on the mass-radius ratio of charged gravitational objects. Our results show that the Buchdahl-Andréasson bound is not saturated. As a result, we see that the proposed model is in good agreement with the stability conditions. Summarizing the results obtained in the present work, within Einstein-Maxwell theory, quark matter in the CFL phase can be potentially used to model stellar structure of relativistic compact objects.

ACKNOWLEDGEMENTS

A. Pradhan thanks to IUCCA, Pune, India for providing facilities under associateship programmes. The author G. P. thanks the Fundação para a Ciência e Tecnologia (FCT), Portugal, for the financial support to the Center for Astrophysics and Gravitation-CENTRA, Insti-

TABLE V. Maximum mass constraints for $1.44M_{\odot}$, $1.6M_{\odot}$ and $2.08M_{\odot}$ based on the choice for the parameters $\Delta = 50$ MeV, $\alpha = 0.695392$ MeV, $B = 70$ MeV/fm³ and $m_s = 150$ MeV, respectively.

M (M_{\odot})	R (Km)	Q ($\times 10^{20}C$)	ϵ_c $\frac{\text{MeV}}{\text{fm}^3}$	$\frac{M}{R}$
1.40	10.12	1.80	412	0.206
1.60	10.43	2.08	432	0.227
2.08	10.99	2.76	529	0.280

tuto Superior Técnico, Universidade de Lisboa, through the Project No. UIDB/00099/2020 and No. PTDC/FIS-AST/28920/2017.

- [1] G. E. Brown and H. A. Bethe, *ApJ*, 423, 659 (1994).
- [2] V. Kalogera and G. Baym, *Astrophys. J. Lett.* **470**, L61 (1996).
- [3] Z. Arzoumanian *et al.* [NANOGrav], *Astrophys. J. Suppl.* **235**, 37 (2018).
- [4] E. Fonseca, *et al.* *Astrophys. J.* **832**, 167 (2016).
- [5] S. N. Zhang *et al.* [eXTP], *Proc. SPIE Int. Soc. Opt. Eng.* **9905**, 99051Q (2016).
- [6] M. C. Miller, *et al.*, *Astrophys. J. Lett.* **887**, L24 (2019).
- [7] T. E. Riley, *et al.*, *Astrophys. J. Lett.* **887**, L21 (2019).
- [8] J. Antoniadis, *et al.*, *Science* **340**, 6131 (2013).
- [9] R. Abbott *et al.* [LIGO Scientific and Virgo], *Astrophys. J. Lett.* **896**, L44 (2020).
- [10] N. B. Zhang and B. A. Li, *Astrophys. J.* **902**, 38 (2020).
- [11] H. T. Wang, S. P. Tang, P. C. Li, M. Z. Han and Y. Z. Fan, *Phys. Rev. D* **104**, 024015 (2021).
- [12] H. Tan, J. Noronha-Hostler and N. Yunes, *Phys. Rev. Lett.* **125**, 261104 (2020).
- [13] A. V. Astashenok, S. Capozziello, S. D. Odintsov and V. K. Oikonomou, *Phys. Lett. B* **811**, 135910 (2020).
- [14] A. V. Astashenok, S. Capozziello, S. D. Odintsov and V. K. Oikonomou, *Phys. Lett. B* **816**, 136222 (2021).
- [15] E. Fonseca, *et al.* *Astrophys. J. Lett.* **915**, L12 (2021).
- [16] T. E. Riley, *et al.*, [arXiv:2105.06980](https://arxiv.org/abs/2105.06980) [astro-ph.HE].
- [17] M. C. Miller, *et al.*, [arXiv:2105.06979](https://arxiv.org/abs/2105.06979) [astro-ph.HE].
- [18] A. Bauswein, *Annals Phys.* **411**, 167958 (2019).
- [19] E. Witten, *Phys. Rev. D* **30**, 272 (1984).
- [20] A. R. Bodmer, *Phys. Rev. D* **4**, 1601 (1971).
- [21] N. Itoh, *PThPh*, **44**, 291 (1970).
- [22] E. Farhi and R. L. Jaffe Strange matter *Phys. Rev. D* **30**, 2379 (1984).
- [23] J. Madsen, *Phys. Rev. D* **47**, 5156 (1993).
- [24] J. Madsen, *Lect. Notes Phys.* **516**, 162 (1999).
- [25] G. Lugones and J. E. Horvath, *Astron. Astrophys.* **403**, 173 (2003).
- [26] R. S. Bogadi, M. Govender and S. Moyo, *Phys. Rev. D* **102**, 043026 (2020).
- [27] M. Matsuzaki and E. Kobayashi, *J. Phys. G* **34**, 1621 (2007).
- [28] M. G. Alford, K. Rajagopal and F. Wilczek, *Phys. Lett. B* **422**, 247-256 (1998)
- [29] C. Anastasiou, L. J. Dixon, K. Melnikov and F. Petriello, *Phys. Rev. D* **69**, 094008 (2004).
- [30] M. Alford and K. Rajagopal, *JHEP* **0206**, 031 (2002).
- [31] A. Steiner, S. Reddy and M. Prakash, *Phys. Rev. D* **66**, 094007 (2002).
- [32] E. A. Becerra-Vergara, S. Mojica, F. D. Lora-Clavijo and A. Cruz-Osorio, *Phys. Rev. D* **100**, 103006 (2019).
- [33] A. Banerjee, T. Tangphati, D. Samart and P. Channuie, *Astrophys. J.* **906**, 114 (2021).
- [34] G. Panotopoulos, T. Tangphati, A. Banerjee and M. K. Jasim, *Phys. Lett. B* **817**, 136330 (2021)
- [35] E. Olson and M. Bailyn *Phys. Rev. D* **12**, 3030 (1975).
- [36] E. Olson and M. Bailyn *Phys. Rev. D* **13**, 2204 (1976).
- [37] J. A. de Diego, D. Dultzin-Hacyan, J. G. Trejo and D. Nunez, [[arXiv:astro-ph/0405237](https://arxiv.org/abs/astro-ph/0405237)] [astro-ph]].
- [38] L. Iorio *Gen. Rel. Grav.* **44**, 1753 (2012).
- [39] C. Alcock, E. Farhi, and A. V. Olinto, *Astrophys. J.* **310** 261 (1986).
- [40] C. Alcock and A. V. Olinto, *Ann. Rev. Nucl. Part. Sci.* **38** 161 (1988).
- [41] J. P. S. Lemos, F. J. Lopes, G. Quinta and V. T. Zanchin, *Eur. Phys. J. C* **75**, 76 (2015).
- [42] J. D. V. Arbañil and V. T. Zanchin, *Phys. Rev. D* **97**, 104045 (2018).
- [43] S. Ray, A. L. Espindola, M. Malheiro, J. P. S. Lemos and V. T. Zanchin, *Phys. Rev. D* **68**, 084004 (2003).
- [44] G. Panotopoulos, T. Tangphati and A. Banerjee, [arXiv:2105.10638](https://arxiv.org/abs/2105.10638) [gr-qc].
- [45] B. V. Ivanov, *Phys. Rev. D* **65**, 104001 (2002).
- [46] V. Varela, F. Rahaman, S. Ray, K. Chakraborty and M. Kalam, *Phys. Rev. D* **82**, 044052 (2010).
- [47] J. Kumar, A. K. Prasad, S. K. Maurya and A. Banerjee, *Eur. Phys. J. C* **78**, 540 (2018).
- [48] A. Nasim and M. Azam, *Eur. Phys. J. C* **78**, 34 (2018).
- [49] S. Thirukkanesh and S. D. Maharaj, *Class. Quant. Grav.* **25**, 235001 (2008).
- [50] G. Panotopoulos and Á. Rincón, *Eur. Phys. J. C* **79**, 524 (2019).
- [51] J. D. V. Arbañil and M. Malheiro, *Phys. Rev. D* **92**, 084009 (2015).
- [52] M. Malheiro, R. Picanco Negreiros, F. Weber and V. Usov, *J. Phys. Conf. Ser.* **312**, 042018 (2011).
- [53] K. Komathiraj and S. D. Maharaj, *Gen. Rel. Grav.* **39**, 2079 (2007).

- [54] P. M. Takisa and S. D. Maharaj, *Gen. Relativ. Gravit.* **45**, 1951 (2013).
- [55] M. Zubair, R. Saleem and M. Lodhi, *Int. J. Geom. Meth. Mod. Phys.* **17**, 2050185 (2020).
- [56] F. Ozel, T. Guver and D. Psaltis, *Astrophys. J.* **693**, 1775 (2009).
- [57] D. J. Nice, E. M. Splaver, I. H. Stairs, O. Loehmer, A. Jessner, M. Kramer and J. M. Cordes, *Astrophys. J.* **634** 1242 (2005).
- [58] J. D. Bekenstein, *Phys. Rev. D* **4**, 2185 (1971).
- [59] F. de Felice, Y. Yu, and Z. Fang, *Mon. Not. R. Astron. Soc.* **277**, L17 (1995).
- [60] J. D. V. Arbañil, J. P. S. Lemos and V. T. Zanchin, *Phys. Rev. D* **88**, 084023 (2013).
- [61] M. G. Alford, *Ann. Rev. Nucl. Part. Sci.* **51**, 131 (2001)
- [62] G. Nardulli, *Riv. Nuovo Cim.* **25N3**, 1 (2002).
- [63] S. Reddy, *Acta Phys. Polon. B* **33**, 4101 (2002).
- [64] M. Alford, K. Rajagopal, S. Reddy, F. Wilczek, *Phys. Rev. D* **64**, 074017 (2001).
- [65] M. Alford and S. Reddy, *Phys. Rev. D* **67**, 074024 (2003).
- [66] G. Lugones and J. E. Horvath, *Phys. Rev. D* **66**, 074017 (2002).
- [67] G. Lugones and J. E. Horvath, *Phys. Rev. D* **66**, 074017 (2002).
- [68] W. P. Alford and B. M. Spicer, *Adv. Nucl. Phys.* **24**, 1 (1998).
- [69] R. Rapp, T. Schafer, E. Shuryak, and M. Velkovsky, *Phys. Rev. Lett.* **81**, 53 (1998).
- [70] E. Farhi and R. L. Jaffe, *Phys. Rev. D* **30**, 2379 (1984).
- [71] C. V. Flores and G. Lugones, *Phys. Rev. C* **95**, 025808 (2017).
- [72] B. K. Harrison, *Gravitational Theory and Gravitational Collapse*, University of Chicago Press, Chicago, 1965.
- [73] Y. B. Zeldovich, and I. D. Novikov, *Relativistic Astrophysics, Vol. I: Stars and Relativity*, University of Chicago Press, Chicago, 1971.
- [74] H. A. Buchdahl, *Phys. Rev.* **116**, 1027 (1959).
- [75] H. Andreasson, *Commun. Math. Phys.* **288**, 715 (2009).
- [76] S. Chakraborty and N. Dadhich, *Phys. Dark Univ.* **30**, 100658 (2020).